# Correlation of primary relaxations and high-frequency modes in supercooled liquids. I. Theoretical background of a nuclear magnetic resonance experiment

B. Geil,[1] G. Diezemann,[2] and R. Böhmer[1]
[1]*Experimentelle Physik III and Interdisziplinäres Zentrum für Magnetische Resonanz, Universität Dortmund, 44221 Dortmund, Germany*
[2]*Institut für Physikalische Chemie, Universität Mainz, 55099 Mainz, Germany*
(Received 24 May 2006; published 30 October 2006)

The question regarding a possible correlation of the time scales of primary and secondary relaxations in supercooled liquids is formulated quantitatively. It is shown how this question can be answered using spin-lattice relaxation weighted stimulated-echo experiments, which are presented in an accompanying paper [A. Nowaczyk, B. Geil, G. Hinze, and R. Böhmer, Phys. Rev. E **74**, 041505 (2006)]. General theoretical expressions relevant for the description of such experiments in the presence of correlation effects are derived. These expressions are analyzed by Monte Carlo integration for various correlation scenarios also including exchange processes, which are the hallmark of dynamical heterogeneity. The results of these numerical simulations provide clear signatures that allow one to distinguish uncorrelated from differently correlated cases. Since modified spin-lattice relaxation effects occur in the presence of nonexponential magnetization recovery, it is shown how to correct for them to a good approximation.

DOI: 10.1103/PhysRevE.74.041504 PACS number(s): 64.70.Pf, 05.40.−a, 76.60.Lz

## I. INTRODUCTION

The complex dynamics of supercooled liquids involves a number of different relaxation processes [1]. The most prominent one is the structural relaxation that accompanies the viscous slow-down. The corresponding molecular motion is characterized by an overall *isotropic* reorientational dynamics as well as by considerable translational displacements [2,3]. In addition to this primary relaxation which is slow near the calorimetric glass transition temperature $T_g$, secondary relaxations are practically always present. In frequency-dependent dielectric measurements of glass-forming systems, they often show up as high-frequency peaks and likewise as the corresponding features in temperature-dependent measurements. One of the important discoveries, reported by Johari and Goldstein in 1970, was that such secondary relaxations are also found in molecularly rigid glass formers and hence in such cases they are not simply a consequence of intramolecular flexibility [4]. A more recent finding is that also supercooled liquids devoid of well-defined Johari-Goldstein (JG) peaks can develop such features out of the so-called excess wing during extended aging experiments close to $T_g$ [5,6]. This conclusion was further vindicated in a rather different approach by using systematic measurements of a series of polyalcohols [7]. In contrast to the primary relaxation, the JG process is characterized by a small-angle dynamics in which the molecules are not performing an isotropic motion [8].

In Fig. 1 we summarize how the various relaxation features typically look in a dielectric loss spectrum of a glass former for which the JG relaxation is not particularly pronounced. This schematic representation leaves open whether or not the excess wing and the JG relaxation stem from the same molecular excitations, a question which is not generally agreed upon in the literature. More relevant in the present context is the fact that important aspects of these relaxation features can be observed using virtually any technique coupling to the structural excitations in the glass former. This holds true even if these techniques operate at essentially a single measuring frequency such as nuclear magnetic resonance (NMR). As an example in Fig. 1 we refer to the spin-lattice relaxation rate $1/T_1$, which can be viewed as being proportional to the loss part of the susceptibility at the Larmor frequency [9,10]. Using spin-lattice relaxation measurements, this loss part is usually, but indirectly [11], mapped out by sweeping external variables such as temperature or pressure [12]. Such approaches assume, however, that the relation between the molecular relaxation frequency, or the inverse correlation time $\tau^{-1}$, and the temperature $T$ (or pressure) is known. Time-temperature equivalence [13], if valid, forms the basis of what is commonly referred to as time-temperature superposition. It is quite often exploited not only in nuclear magnetic resonance (NMR) but also in, e.g., mechanical spectroscopy [14].

There are only few experimental data [15,16] and theoretical considerations [17] directly addressing a correlation of the different motional processes. This may appear surprising in view of the fact that various experimental observations are available that may be linked to this question. In an early experiment, Williams [18] reported that upon the application of pressure to a supercooled polymer the strength of its $\alpha$ relaxation increases at the expense of that of the $\beta$ process. This and other observations [19], e.g., that in the glassy state the strength of the $\beta$ process in small-molecule glass formers depends on the thermal cooling history [4], suggest that the two processes are in some way linked with one another.

One of the purposes of the present work is to address most directly the extent to which $\alpha$ and $\beta$ relaxations may be correlated in viscous liquids, by drawing upon the knowledge that the primary [20–23] as well as the secondary processes [24–26] exhibit a heterogeneous dynamics. This implies the existence of a distribution of correlation times. Consequently we are allowed to associate distributions of

 

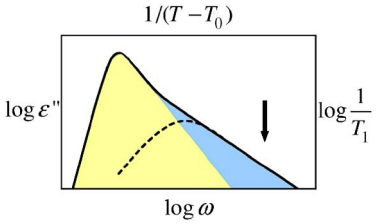


FIG. 1. (Color online) Schematic dielectric loss spectrum $\varepsilon''(\omega)$ (lower and left axes) adapted from Lunkenheimer *et al.* [5]. The main peak is a sketch of the primary relaxation while the additional contributions at high frequencies are meant to correspond to the so-called excess wing. Reference [5] provides also a sketch for a glass former with a more pronounced JG process, which here is indicated by the dashed line. Information similar to that provided by $\varepsilon''(\omega)$ may be obtained from the measurement of $1/T_1$ at a single frequency (upper and right axes) if the temperature axis is properly scaled. Using the considerations of, e.g., Refs. [9,10] one may define the dielectric analog of a spin-lattice relaxation rate via $1/T_1^{\mathrm{diel}} \propto [\varepsilon''(\omega_L)+4\varepsilon''(2\omega_L)]/(\omega_L \Delta\varepsilon)$ if details such as the different angular sensitivities of dielectric and NMR experiments are disregarded. In the above equation $\Delta\varepsilon$ designates the amplitude of the dielectric relaxation strength. The arrow in the figure is meant to provide a rough but experimentally relevant indication of the relation of the Larmor frequency relative to the dielectric loss peak near $T_g$.

correlation times $G(\tau)$ with data such as the one sketched in Fig. 1.

This paper is organized as follows: First, in Sec. II, we describe the idea leading to an NMR experiment which simultaneously is sensitive on short- *and* on long-time scales. Then, in Sec. III, we discuss the occurrence of a modified spin-lattice relaxation in these experiments and outline a useful approximate correction. In Sec. IV we derive some general theoretical analytical expressions relevant for the description of our results in the presence of correlation effects. This is followed, in Sec. V, by numerical simulations implementing these expressions and generalizations thereof, including dynamical exchange processes. Finally, we discuss various correlation scenarios for the comparison with experimental results (that will be presented in Ref. [27], see also Ref. [28]) and then summarize our main findings in Sec. VI.

## II. PRINCIPLES OF SPIN-RELAXATION WEIGHTED STIMULATED-ECHO SPECTROSCOPY

To illustrate the idea on which our present experiment is based, distributions of $\alpha$ and $\beta$ relaxation times are plotted in a schematic fashion along two orthogonal axes in Fig. 2. This two-dimensional representation allows us to visualize possible correlations among various parts of the distributions in a simplifying fashion. Taking, for the time being, the parts of the distributions as discrete quantities possible correlations among them can be expressed by marking the corresponding box in the grid as sketched in Fig. 2. In the more quantitative description that we will provide further below, this picture will be helpful in defining a correlation matrix. One of the most interesting questions in this context is whether and then how the entries of such a matrix should be chosen. Various qualitatively different scenarios are possible. A description of independent relaxation processes may be achieved by choosing the matrix elements in a random fashion. Correlated scenarios include the one depicted in Fig. 2 in which the "diagonal" curve connects the slow part of the $\beta$ distribution with the slow part of the $\alpha$ distribution. Of course, one may also envision that slow contributions of the $\alpha$ distribution are connected with the fast parts of the $\beta$ distribution in an "antidiagonal" way.

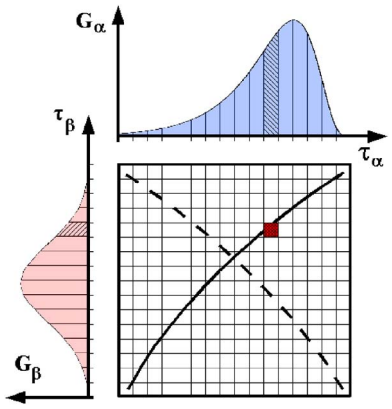


FIG. 2. (Color online) Schematic distributions of correlation times for a glass-former exhibiting $\alpha$ and $\beta$ relaxations are plotted on two orthogonal axes. The filled square in the grid provides a means to indicate that some part of the $\alpha$ spectrum is connected with some part of the $\beta$ spectrum. The curved line indicates but one possible scenario for which the connectivity spans the entire distributions. The distributions corresponding to the $\alpha$ and the $\beta$ process are drawn separately because they correspond to different prefactors $K$ [cf. Eq. (1)], even when referring to the same correlation time.

### A. Sensitivity to fast motions

Obviously an experimental method is needed which is sensitive on the scale of the primary as well as on that of the secondary relaxation. In principle measurements of spin-lattice relaxation times $T_1$ can provide such a global sensitivity. This is because $1/T_1$ is proportional to the fluctuation amplitude characterizing the molecular motion (more precisely the corresponding nuclear interaction tensor) at some frequency $\omega$. However, in conventional NMR experiments the fluctuation spectrum, also called spectral density $J(\omega)$, is probed at a single frequency, the Larmor frequency $\omega_L$. It turns out that the spin-lattice relaxation rate, here written as

$$\frac{1}{T_1} = K[J(\omega_L) + 4J(2\omega_L)], \tag{1}$$

is most sensitive to time scales $\tau \approx 0.61/\omega_L$ [29], which for typically used external magnetic fields corresponds to a few nanoseconds. However, if the nuclear coupling constant $K$ [30] and the spectral form of $G(\tau)$ and hence $J(\omega_L)$ are known, then $T_1$ can be computed. In the so-called slow-

motion regime $\omega_L \tau \gg 1$, i.e., for temperatures far below the $T_1$ minimum, Eq. (1) reduces to [31]

$$\frac{1}{T_1} = \frac{4K}{5\omega^2 \tau}. \tag{2}$$

This means that under these circumstances spin-lattice relaxation times and molecular correlation times are proportional to one another. Typical deuteron coupling constants $K$, which can be estimated from the width of the corresponding NMR spectra, are of the order of $(2\pi \times 0.1\ \mathrm{MHz})^2$. Taking $\omega_L = 2\pi \times 100$ MHz, it is clear that the proportionality constant $4K/(5\omega_L^2)$ in Eq. (2) is of the order of $10^{-6}$. In other words, molecular dynamics taking place on a time scale of a few microseconds under circumstances implied by Eq. (2) lead to spin-lattice relaxation times of the order of a few seconds [32]. Primary correlation times of the order of seconds or longer would thus correspond to $T_1$ being much longer than experimentally observed. This argument shows that close to $T_g$ spin-lattice relaxation cannot be dominated by the $\alpha$ process under these circumstances.

Unfortunately the contributions to $T_1$ originating from different parts of a distribution function cannot, in general, be disentangled in a straightforward manner. However, in appropriate temperature ranges (cf. the arrow in Fig. 1), the contribution of the primary relaxation to $1/T_1$ is reduced by typically one to three orders of magnitude with respect to that of the secondary processes. It is in this temperature regime in which the heterogeneity of the $\beta$-process could be identified as follows. It is theoretically well established that each ensemble of dynamically equivalent deuterons (commonly termed isochromat), relaxes in a single-exponential manner [33], i.e., with a longitudinal relaxation rate $R_1$. Thus the experimental observation, made using deuteron NMR [24,34], that the longitudinal nuclear magnetization $M(t)$ recovered in a nonexponential fashion implies the existence of a distribution of spin-lattice relaxation times and thus a distribution of secondary relaxation times. Due to the former, the properly normalized time dependence of the nonexponentially relaxing magnetization can be written as

$$M(t) = \int_0^\infty V(T_1) e^{-t/T_1} dT_1 = \int_0^\infty P_{1|0}(R_1) e^{-R_1 t} dR_1. \tag{3}$$

Here $V(T_1)$ designates the normalized distribution of spin-lattice relaxation times in a heterogeneous sample. On the right hand side of Eq. (3), we give an equivalent formulation using the *a priori* probability $P_{1|0}(R_1)$ in terms of van Kampen's notation [35]. $P_{1|0}(R_1)$ reflects the unfiltered distribution of spin-lattice relaxation rates $R_1$. The time dependence experimentally observed for $M(t)$ can often be described excellently by the empirical stretched-exponential function

$$M(t) = \exp[-(t/T_1)^{1-\nu}], \tag{4}$$

using the stretching exponent $\nu$. In this case, the first moment of $V(T_1)$ is given by

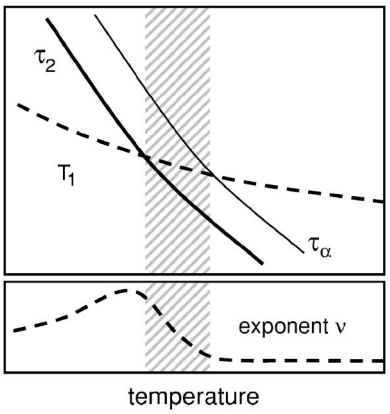


FIG. 3. Sensitivity to the *distribution* of secondary relaxation times is only possible for $\nu > 0$. However, the low-temperature limit of the present technique will usually not be given by the onset of spin-diffusion which leads to a decrease of $\nu$, but by the condition $\tau_2 \approx T_1$ [here $\tau_2$ is the time scale on which the orientational correlation function, Eq. (7), decays]. This is because if $\tau_2 \gg T_1$ then $\tau_2$ can not be determined reliably from (noisy) experimental data. These constraints result in a quite small useful temperature range, which is marked here by the shaded area. In this range $\tau_2$ and the primary relaxation time $\tau_\alpha$ will exhibit the same temperature dependence.

$$\langle T_1 \rangle = \int_0^\infty M(t) dt = \frac{T_1}{1-\nu} \Gamma\left(\frac{1}{1-\nu}\right). \tag{5}$$

Note that a $T_1$ distribution (here parametrized by $\nu > 0$) can only be observed if the average relaxation time $\langle T_1 \rangle$ is shorter than the primary relaxation time. If this is not the case, i.e., if $\tau_\alpha \gg \langle T_1 \rangle$, then dynamic exchange processes within the $T_1$ distribution restore ergodicity. Such exchange processes were directly observed using reduced four-dimensional NMR and similar techniques [20,36]. It is important to keep in mind that the same dynamic exchange processes are relevant [37] for the primary relaxations *and* for the spin-lattice relaxations [24,38]. The consequent averaging of the magnetization recovery, resulting from an efficient exchange, can be recognized from $\nu \approx 0$.

The temperature dependence of $\nu$ as it is typical for supercooled liquids is shown in Fig. 3 in a schematic fashion. At high temperatures, dynamical averaging leads to $\nu \approx 0$ down to about the point at which the strongly temperature-dependent trace of the primary relaxation time $\tau_\alpha$ crosses that of $T_1$. The relatively weak temperature variation of $T_1$ essentially reflects that of $\tau_\beta$ in the sketched temperature range. For lower temperatures for which averaging becomes less effective, $\nu$ first increases until spin-diffusion sets in and then renders the magnetization recovery more and more exponential [39]. Thus, the sensitivity of the spin-relaxation experiment for secondary relaxations can only be exploited in the narrow temperature range marked by the shading in Fig. 3.

### B. Combination with slow motions

In order to be able to extract information about a possible connection of primary and secondary relaxation processes,

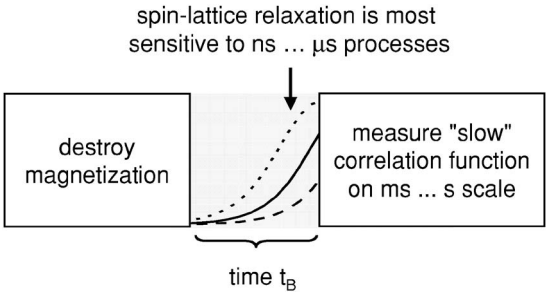


FIG. 4. The spin-relaxation weighted stimulated-echo spectroscopy has the structure of a pump (or modify or select), wait, and probe experiment. In its first part, the magnetization is destroyed using a saturation sequence; in the second part, each magnetization isochromat can build up with its own rate and enter the third part with the amplitude it has reached at the end of the time interval $t_B$. Finally, in the third part, the rotational decorrelation of the various isochromats is measured with the weighting acquired during $t_B$. In the limit $t_B \gg \langle T_1 \rangle$ the conventional rotational correlation function is recovered.

we may combine the spin-relaxation experiment with a technique which is sensitive to the slow dynamics, e.g., following the scheme outlined in Fig. 4. In the first part of the experiment, sketched there, a nonequilibrium magnetization state is created, in our case by employing a saturation sequence [40] in order to destroy the total magnetization. During the subsequent time interval $t_B$, the various magnetization components associated with $V(T_1)$ will build up again at various rates. According to Eq. (2) those components characterized by the fastest correlation times will recover most rapidly. If the build-up interval is sufficiently long, then all magnetization components will enter the subsequent detection block with their proper weight given by $V(T_1)$. However, if $t_B < \langle T_1 \rangle$, as sketched in Fig. 4, those molecules with the shortest $T_1$ will contribute most to the subsequently detected signal. The magnetization at the end of the time interval $t_B$, i.e., the one which enters the second part of the experiment, reflects a modified distribution of rates,

$$P^*_{1|0}(R_1,t_B) = [1 - \exp(-R_1 t_B)] P_{1|0}(R_1). \tag{6}$$

The main advantage of the experimental protocol, on which the present theoretical analysis is based, arises from the ability to study the primary process in the second part of the experiment, however, starting from *different* initial conditions. The latter are adjusted by the time interval $t_B$ and hence by an accordingly filtered distribution of spin-lattice relaxation rates which in turn depend on the secondary processes.

In order to monitor the ultraslow motions associated with the primary relaxation, one could, e.g., measure absorption spectra [41] or, as we do in the present work, rotational correlation functions involving the quadrupolarly perturbed precession frequencies $\omega_Q(t) = \frac{1}{2}\delta_Q [\, 3\cos^2\theta(t) - 1)]$. The latter depend on the molecular orientation as characterized by the polar angle $\theta$ in the usual fashion. Furthermore, the anisotropy parameter $\delta_Q = (3/4)(e^2 qQ/\hbar)$ is proportional to the square root of the coupling constant $K$. Two-time autocorrelation functions involving $\omega_Q(t)$ were measured using a three-pulse stimulated-echo sequence. In the limit $t_B \to \infty$ or without any initial saturation these functions were extensively discussed in the literature [2,42]. The cosine variant which is employed here may be written as

$$F_2(t_p,t_m) = \langle \cos[\omega_Q(0)t_p] \cos[\omega_Q(t_m)t_p] \rangle, \tag{7}$$

if we neglect spin-relaxation effects. Here the angle brackets indicate the ensemble (and powder) average, $t_m$ designates the mixing time. The evolution time $t_p$ is an experimentally adjustable parameter which governs the angular sensitivity of the measurement [2]. The stimulated-echo technique was often used to extract motional correlation times in the range spanning from about milliseconds to seconds. The decay time of the cos-cos function appearing in Eq. (7) will be called here $\tau_2$. For supercooled liquids $\tau_2$ is closely related to $\tau_\alpha$ and distributions of $\tau_2$ reflect the ones in $\tau_\alpha$. We restrict ourselves to relatively large evolution times for which $\tau_2$ is practically independent of $t_p$ and each angular jump leads to a complete loss of correlation [43]. In this limit the average $\tau_2$ is smaller than the average $\tau_\alpha$. This fact, which is due to the presence of relatively small jump angles in supercooled liquids, is also schematically incorporated in Fig. 3.

In supercooled liquids $F_2$ typically follows a stretched exponential form. In various previous experiments on a host of different disordered systems, it was shown that stretched-exponential behavior arises from dynamically distinguishable subensembles [44]. In the presence of a heterogeneous scenario, one may characterize each isochromat in viscous liquids by an exponential function [45].

In Eq. (7) the spin-relaxations occurring during $t_p$ and during $t_m$ were neglected. To our knowledge heretofore they were only introduced as additional, empirical damping factors so that the right-hand side of Eq. (7) reads

$$F_2(t_p,t_m) = \langle \cos[\omega_Q(0)t_p] \cos[\omega_Q(t_m)t_p] \rangle \times \exp(-t_m/T_1) \exp(-2t_p/T_2), \tag{8}$$

if we choose to write the damping factors as exponential decays. Since in the accompanying experimental paper [27] all measurements are performed at constant $t_p$, the damping due to the spin-spin relaxation, parameterized here by $T_2$, is a constant factor which we will not consider further.

The factorization of the correlation and the damping terms expressed by Eq. (8) implies either that spin-lattice relaxation is exponential, as is the case for most stimulated-echo experiments reported in the literature [46], or that primary and secondary (and hence spin-lattice) relaxation times are uncorrelated. Since our experiments are designed to check whether or not such correlations exist, we cannot *a priori* use the factorization implied by Eq. (8). Situations in which correlations exist are treated in Sec. IV, below.

Before closing this section we note that it is possible to turn the spin-lattice relaxation weighted stimulated-echo experiment upside down. This means that one can first select slow contributions to the primary relaxation using the stimulated-echo sequence and then probe their spin-lattice relaxation. In fact, such an experiment was performed some time ago for amorphous polystyrene [15]. It was suggested

that different effective spin-relaxation times could be measured if the primary relaxation was low-pass filtered to different extents [47].

## III. CORRECTION FOR MODIFIED SPIN-LATTICE RELAXATION

It is important to realize that the spin-lattice relaxation filter described above has an effect on the subsequent decay of the stimulated-echo decay, which takes place during the mixing time $t_m$ even if primary and secondary relaxations are *un*correlated. Why this is so is most easily explained by assuming that during the mixing time the quadrupolar frequencies in Eq. (7) do not change [48] so that only spin-relaxation effects need to be considered. In the present section we will adhere to this assumption for the sake of simplicity.

Via Eq. (6) the magnetization at the end of the build-up time is due to a modified distribution of spin-lattice relaxation rates $P^*_{1|0}(R_1,t_B)=[1-\exp(-R_1t_B)]P_{1|0}(R_1)$. In analogy to Eq. (3), this gives rise to a modified spin-lattice relaxation function

$$M^*(t_B,t_m)=\int_0^\infty [1-\exp(-R_1t_B)]P_{1|0}(R_1)\exp(-R_1t_m)dR_1. \tag{9}$$

In the absence of molecular dynamics, this integral immediately yields a relaxation factor

$$M^*(t_B,t_m)=M(t_m)-M(t_B+t_m). \tag{10}$$

It is important to realize that it is not necessary to know the distribution of spin-lattice relaxation rates $P_{1|0}(R_1)$ to compute $M^*$. Equation (10) shows how $M^*$ can be determined from the independently measured spin-lattice relaxation function $M(t)$. In the presence of noise, i.e., when dealing with experimental data, this determination has to be done with great care. This is because $M(t_m)$ and $M(t_B+t_m)$ will be similar in magnitude for specific combinations of $t_m$ and $t_B$ and therefore the difference of the two quantities is *very* sensitive to experimental uncertainties.

Equation (10) is instructive for situations in which the correlation and the damping terms factorize [cf. Eq. (8)]. However, it is not clear to what extent it continues to hold strictly if this simplification ceases to be applicable, e.g., when primary and secondary relaxations *are* correlated. Also in view of the discussion given in Sec. V B below, even in this situation Eq. (10) should be considered as a very useful, albeit *approximate* correction when trying to remove spin-relaxation effects from the experimental data that we will present in Ref. [27].

## IV. GENERAL THEORETICAL CONSIDERATIONS

For a more detailed theoretical treatment of the current spin-lattice relaxation weighted stimulated-echo experiment, it is convenient to start from a general description of the echo amplitude function including correlation effects. In the corresponding experimental functions, which above were called $F_2$, all possible correlations, dynamical exchange processes, etc. are automatically included if present in the sample under examination. For the theoretical functions, on the other hand, it is clearly defined which effects are included and we will use the symbol

$$S(t_B,t_p,t_m)=\int d\omega_1\int d\omega_2\int d\tau_C\int dR_1P_{4|0}(\omega_1,\omega_2,\tau_C,R_1)\times\cos(\omega_1t_p)\cos(\omega_2t_p)[1-\exp(-R_1t_B)]\times\exp(-R_1t_m). \tag{11}$$

to denote a stimulated-echo function in this context. This function depends on the four stochastic variables $\omega_1=\omega_Q(0)$, $\omega_2=\omega_Q(t_m)$, $\tau_C$, and $R_1$. The latter two quantities denote a correlation time $\tau_C$ and the spin-lattice relaxation rate $R_1$, respectively. It is important to point out that in the present context each quantity characterizes an individual isochromat and it is understood that $\tau_C$ is a measure of the time scale of the $\alpha$ process and $R_1$ is related to the time scale of the $\beta$ process.

Furthermore, in order to compute the ensemble average via the fourfold integral, we introduced the fourth-order joint probability density $P_{4|0}(\omega_1,\omega_2,\tau_C,R_1)$ of finding $\omega_Q(0)$ between $\omega_1$ and $\omega_1+d\omega_1$, $\omega_Q(t_m)$ between $\omega_2$ and $\omega_2+d\omega_2$, and analogously for $\tau_C$ and $R_1$. Note that the spin-relaxation effects, in the form $\exp(-R_1t_m)-\exp[-R_1(t_B+t_m)]$ [cf. Eq. (10)], are now *included* in the ensemble average. In the following, we will discuss a few special cases of the general expression, Eq. (11), which facilitate a relatively simple theoretical treatment.

### A. The uncorrelated case

If we assume that $\tau_C$ and $R_1$, and hence $\tau_\alpha$ and $\tau_\beta$, are *uncorrelated*, then we can factorize $P_{4|0}(\omega_1,\omega_2,\tau_C,R_1)=P_{3|0}(\omega_1,\omega_2,\tau_C)\,P_{1|0}(R_1)$. Under these conditions, Eq. (11) becomes

$$S(t_B,t_p,t_m)=\int d\omega_1\int d\omega_2\int d\tau_CP_{3|0}(\omega_1,\omega_2,\tau_C)\cos(\omega_1t_p)\times\cos(\omega_2t_p)\int dR_1P_{1|0}(R_1)[1-\exp(-R_1t_B)]\times\exp(-R_1t_m). \tag{12}$$

In the absence of spin-lattice relaxation, $R_1\to0$, this expression reduces to Eq. (7).

If exchange processes are absent, we may use Bayes' rule to split the joint probability $P_{3|0}(\omega_1,\omega_2,\tau_C)=P_{2|1}(\omega_1,\omega_2|\tau_C)P_{1|0}(\tau_C)$ into the *a priori* probability $P_{1|0}(\tau_C)$ [49] and into the conditional probability $P_{2|1}(\omega_1,\omega_2|\tau_C)$ of finding $\omega_1$ and $\omega_2$ under the assumption that the correlation time has the value $\tau_C$. In the context of two-dimensional NMR, the probability $P_{2|1}(\omega_1,\omega_2|\tau_C)$ has been thoroughly investigated [50]. It is also useful when computing the two-time stimulated echo function $S_2$ for a single, well-defined $\tau_C$, e.g., by writing

$$S_2(t_p,t_m;\tau_C) = \int d\omega_1 \int d\omega_2 P_{2|1}(\omega_1,\omega_2|\tau_C) \times \cos(\omega_1 t_p)\cos(\omega_2 t_p), \quad (13)$$

and by performing the necessary integration over the distribution of correlation times afterwards.

### B. Simple correlation scenarios

In the general case, when $\tau_C$ and $R_1$ could be correlated, $P_{4|0}$ does not necessarily factorize into lower-order joint probabilities. But we may again use Bayes' rule to obtain [51]

$$P_{4|0}(\omega_1,\omega_2,\tau_C,R_1) = P_{2|2}(\omega_1,\omega_2|\tau_C,R_1)P_{1|1}(\tau_C|R_1)P_{1|0}(R_1). \quad (14)$$

Here $P_{1|1}(\tau_C|R_1)$ expresses in a well-defined way the connection between $\tau_C$ and $R_1$. $P_{1|1}(\tau_C|R_1)$ can be regarded as the continuous form of what in connection with Fig. 2 was alluded to as the correlation matrix. For simplicity we assume that $R_1=f(\tau_C)$ is a deterministic (rather than a stochastic) function of $\tau_C$ such that

$$P_{1|1}(\tau_C|R_1) = \delta[\tau_C - f^{-1}(R_1)], \quad (15)$$

where $\delta$ is Dirac's delta function. For correlated scenarios $P_{1|0}(\tau_C)$ and $P_{1|0}(R_1)$ can mutually be expressed by one another. If $R_1=f(\tau_C)$ is a monotonous function, then the transformation connecting the two distributions is simply given by $P_{1|0}(R_1)dR_1=P_{1|0}(\tau_C)d\tau_C$. In general, however, we have to sum over the $n$ monotonous segments of $f(\tau_C)$ so that the transformation can be written as

$$P_{1|0}(R_1) = \sum_n P_{1|0}(\tau_C)\left|\frac{df(\tau_C)}{d\tau_C}\right|^{-1}_{\tau_C^{(n)}=f_n^{-1}(R_1)}. \quad (16)$$

Here $f_n^{-1}(R_1)$ is the $n$th (real) root of $f(\tau_C)-R_1=0$ and the summation is performed over all of these roots. Inserting Eqs. (14)–(16) into Eq. (11) after integration over $R_1$ yields

$$S^*(t_B,t_p,t_m) = \int d\tau_C \int d\omega_1 \int d\omega_2 P_{2|1}(\omega_1,\omega_2|\tau_C)\cos(\omega_1 t_p) \times \cos(\omega_2 t_p)[1-\exp(-f(\tau_C)t_B)]\exp(-f(\tau_C)t_m) \times \sum_n P_{1|0}(\tau_C)\left|\frac{df(\tau_C)}{d\tau_C}\right|^{-1}_{\tau_C^{(n)}=f_n^{-1}(R_1)}. \quad (17)$$

In order to evaluate this expression, we will use the simplifying assumptions (i) that the subintegrals $S_2(\omega_1,\omega_2;\tau_C)$ [cf. Eq. (13)] appearing indirectly in Eq. (17) decay exponentially for a suitably chosen subensemble and (ii) that the spin-lattice relaxation of a suitably chosen subensemble proceeds exponentially as well. Then for certain distribution functions $P_{1|0}(\tau_C)$ and certain functional forms for $f(\tau_C)$ Eq. (17) may be solved analytically if exchange processes are absent. To allow for a larger flexibility, in the following section we will solve Eq. (17) by numerical Monte Carlo integration. Among the scenarios we treat are the functions

$$f(\tau_C) = \begin{cases} f_C/\tau_C & \text{positive correlation} \\ f_A\tau_C & \text{negative correlation} \end{cases}, \quad (18)$$

which connect $\tau_C$ and $f(\tau_C)=R_1$. In the last equation $f$ has been assumed to take a very simple form involving the factors $f_C$ and $f_A$ [52]. More complicated scenarios will be considered below.

## V. STOCHASTIC SIMULATIONS

In this section we will provide details concerning the numerical implementation of the above considerations. In addition, the simulation presented here allows us to include the effect of dynamical exchange effects in a relatively simple fashion. By dynamical exchange processes, we mean that a given particle, or a suitably chosen isochromat, can change its time constant $\tau_C$ within the distribution of correlation times, $P_{1|0}(\tau_C)$, and likewise $R_1$ can change within its distribution, $P_{1|0}(R_1)$. As noted above, the primary as well as the spin relaxation are governed by the *same* exchange process. Therefore, these exchange processes are not only defined by the same exchange rate, $\kappa$, but in our simulations they will also take place simultaneously.

In the experiments the buildup of the magnetization that follows the saturation is most conveniently described by a distribution of spin-lattice relaxation times $T_1$ rather than by a distribution of rates $R_1$ [38]. Consequently, in order to mimic the experimental situation as closely as possible, the simulations will be formulated in terms of $P_{1|0}(T_1)$ rather than of $P_{1|0}(R_1)$.

### A. Algorithm

For the simulation of dynamic exchange processes, we consider a large number $N$ of isochromats. Like above, we call an ensemble of dynamically equivalent particles, spins, etc. an isochromat. For the purpose of our simulations, we will consider the isochromats, numbered by the index $k$, as a stochastic process $\xi^{(k)}(t)=[\tau_C^{(k)}(t),T_1^{(k)}(t)]$. This means that at a given time the state $\xi^{(k)}(t)$ is defined by the two variables $\tau_C^{(k)}$ and $T_1^{(k)}$. The first of them characterizes the time constant of the $\alpha$ process and the second is related with the time constant of the $\beta$ process. Furthermore, we assume that the state variable $\xi^{(k)}(t)$ changes discontinuously at discrete points in time given by $t_i^{(k)} \in \{t_0^{(k)}=0,t_1^{(k)},\ldots,t_\ell^{(k)}\}$. Hence the lifetime of a state, which is subject to an exchange process, is $\Delta t_i^{(k)}=t_i^{(k)}-t_{i-1}^{(k)}$. During the $i$th lifetime of a state, the value of $\tau_C^{(k)}$ and $T_1^{(k)}$ are *constant* and denoted as $\tau_{C,i}^{(k)}$ and $T_{1,i}^{(k)}$, respectively. Assuming that the exchange process is Markovian, the corresponding distribution of lifetimes is $L(\Delta t)=\kappa\exp(-\kappa\Delta t)$ [35]. Note that these exchange processes have no effect on the decay of the orientational correlation function in our simulations, since in the chosen algorithm the exchange does not affect the orientational motion at all.

In Fig. 5 we sketch the trajectory of an isochromat. Whenever the temporary lifetime of a state expires, i.e., at the time $t_i^{(k)}$, a new random life time is chosen from $L(\Delta t)$ and new

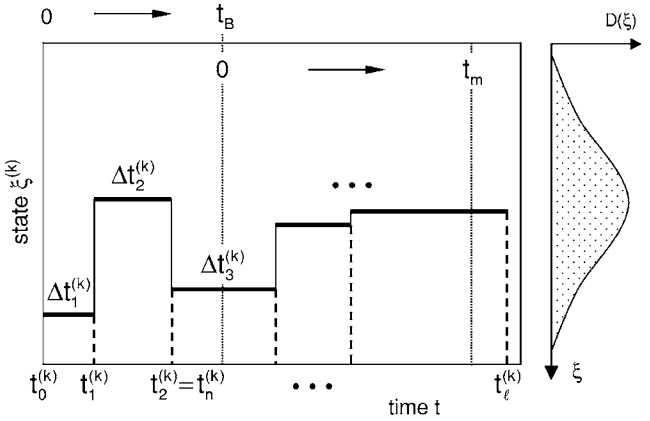


FIG. 5. Sketch of a trajectory of an isochromat $k$. The two-dimensional state variable $\xi(t)=(\tau_C(t),T_1(t))$ and the corresponding two-dimensional distribution $D(\xi)$ from which $\xi$ is drawn are depicted in a simple one-dimensional representation. In the present figure $D(\xi)$ is meant to represent the distribution of all isochromats.

values $\tau_{C,i+1}^{(k)}$ and $T_{1,i+1}^{(k)}$ are drawn from the corresponding distributions $P_{1|0}(\tau_C)$ and $P_{1|0}(T_1)$. If from these distributions $\tau_{C,i+1}^{(k)}$ and $T_{1,i+1}^{(k)}$ are chosen independent of one another, one obtains what above was called the uncorrelated case. Correlated scenarios arise if the choice of one of the variables fixes the other one, completely or at least to some extent.

Using trajectories such as those depicted in Fig. 5, we can construct the nuclear polarization of each isochromat during the time intervals $t_B$ and $t_m$. For $0<t\leqslant t_B$ the only change in spin polarization originates from the recovery of the equilibrium magnetization via $T_1$ relaxation. Within the time interval $\Delta t_i$ the state of the $k$th isochromat is then characterized by the constant value $T_{1,i}^{(k)}$ and, as above, we assume that the polarization of a single isochromat is acquired exponentially, i.e., its change is proportional to $\exp(-t/T_{1,n}^{(k)})$. Thus in the time interval $t_n^{(k)}<t\leqslant t_{n+1}^{(k)}$, the $k$th isochromat accumulates a polarization $\exp[-(t-t_n^{(k)})/T_{1,n+1}^{(k)}]$ and the total polarization accumulated from the beginning of the experiment is

$$p_0^{(k)}(t)=1-\left\{\prod_{i=1}^{n}\exp[-\Delta t_i^{(k)}/T_{1,i}^{(k)}]\right\}\exp[-(t-t_n^{(k)})/T_{1,n+1}^{(k)}]. \tag{19}$$

Equation (19) is valid as long as $t\leqslant t_B$. At the end of the build-up time, the polarization $p_0^{(k)}(t_B)$ is obtained which is used as the starting polarization of the $k$th isochromat in the second part of the simulation, i.e., during the mixing time $t_m$. In this part we have to implement not a build up but a *decay* of the nuclear polarization due to spin-lattice relaxation and more importantly we have to include the effect of the $\alpha$ relaxation. In accord with the conventions used in the experimental protocol, the time variable $t$ is restarted at the beginning of the mixing time. Therefore during the fraction of $\Delta t_n^{(k)}$ which ranges from the end of the build-up interval into the mixing interval the polarization decays with

$$p^{(k)}(t)=p_0^{(k)}(t_B)\exp(-t/T_{1,n+1}^{(k)})\exp(-t/\tau_{C,n+1}^{(k)}). \tag{20}$$

Since we focus on relatively large evolution times, $\tau_{C,i}^{(k)}$ may be interpreted as the effective decay time of the orientational correlation function. Therefore the decay in each interval may be characterized by an exponential decay.

As illustrated in Fig. 5, we used a consecutive numbering of the time *intervals* throughout the entire simulation protocol. Hence, in general, we can write the polarization during $t_m$ as

$$p^{(k)}(t)=p_0^{(k)}(t_B)p_{T_1}^{(k)}(t)p_{\tau_C}^{(k)}(t) \tag{21a}$$

with

$$p_{T_1}^{(k)}(t)=\exp[-(t_{n+1}^{(k)}-t_B)/T_{1,n+1}^{(k)}]\left\{\prod_{i=n+1}^{\ell}\exp[-\Delta t_i^{(k)}/T_{1,i}^{(k)}]\right\}\times\exp[-(t+t_B-t_\ell^{(k)})/T_{1,\ell}^{(k)}] \tag{21b}$$

and

$$p_{\tau_C}^{(k)}(t)=\exp[-(t_{n+1}^{(k)}-t_B)/\tau_{C,n+1}^{(k)}]\left\{\prod_{i=n+1}^{\ell}\exp[-\Delta t_i^{(k)}/\tau_{C,i}^{(k)}]\right\}\times\exp[-(t+t_B-t_\ell^{(k)})/\tau_{C,\ell}^{(k)}]. \tag{21c}$$

Here, in addition to the first, the last time interval $\Delta t_\ell^{(k)}$ is also singled out of the product, since in general it can terminate after the mixing time is over (cf. Fig. 5). In Eqs. (21), one notes the complete analogy of the terms $\tau_{C,i}^{(k)}$ describing the primary process with those containing $T_{1,i}^{(k)}$ relating to the spin-lattice relaxation. Of course also during the entire build-up interval $t_B$ the state variable $\xi^{(k)}(t)$ contains information about the $\alpha$-relaxation. However, since during $t_B$ the $\tau_{C,i}^{(k)}$ relaxation is irrelevant for the current experiment the exponential terms containing $\tau_{C,i}^{(k)}$ have not been included in Eq. (19).

### B. Simulation results

The computations were carried out for typically $N=10^5$ isochromats and we subsequently averaged the nuclear polarization curve for the build-up as well as for the mixing times. At this stage, this gives us a set of data which can be analyzed in full analogy to the experimental results. However, based on the simulation, we can additionally disentangle the various decays contributing to the total nuclear polarization, i.e.,

$$\langle p_{T_1}(t)\rangle=\frac{1}{N}\sum_k p_{T_1}^{(k)}(t) \tag{22a}$$

and

$$\langle p_{\tau_C}(t)\rangle=\frac{1}{N}\sum_k p_{\tau_C}^{(k)}(t) \tag{22b}$$

[cf. Eq. (21)]. Note that these functions are accessible via simulations but not from NMR data obtained in a laboratory experiment. Thus we can analyze separately the part stemming from the spin-lattice decay as well as analyze

separately the loss of orientational correlation, at least in the case of the uncorrelated scenario. Furthermore, we can implement various connectivities between $T_1$ and $\tau_C$ and thus learn if and how the effective correlation times $\tau_2$ depend on $t_B$.

In order to mimic the situation in glass-forming systems, we chose broad distributions of $\tau_C$ and $T_1$ which are best represented on a logarithmic time scale. The shape of such distributions is not known in detail from experimental data and thus for convenience we decided to work with distributions which are constant on a logarithmic time scale, i.e.,

$$P_{1|0}(\ln \tau_C) = \begin{cases} \text{const} & \text{for } 10^1 \text{ s} < \tau_C < 10^3 \text{ s} \\ 0 & \text{otherwise} \end{cases} \quad (23a)$$

and

$$P_{1|0}(\ln T_1) = \begin{cases} \text{const} & \text{for } 10^2 \text{ s} < T_1 < 10^4 \text{ s} \\ 0 & \text{otherwise} \end{cases} \quad (23b)$$

On a linear scale, these distributions would appear with a strongly asymmetric shape. Consequently the average time scales are longer than corresponding to the middle of the intervals just given. The parameter ranges chosen here roughly correspond to typical experimental values. It was checked that the modified spin-lattice relaxation, $\langle p_{T_1}(t)\rangle$, as calculated using Eq. (22a) is indeed identical to what is expected from $M^*(t)$ [cf. Eq. (10)] if the uncorrelated scenario is assumed. It should be recalled that for correlated scenarios the modified spin-lattice relaxation is only accessible in the simulations and not in the experiment. Likewise, the modified correlation function, Eq. (22b), is not available from experimental data.

In Figs. 6 and 7, we summarize the results of simulations that were obtained for several scenarios. First we checked numerically that $\tau_2$ is independent on $t_B$ for the uncorrelated scenario. This is expected because the total polarization

$$\langle p(t)\rangle = \frac{1}{N}\sum_k p_{T_1}^{(k)}(t) p_{\tau_C}^{(k)}(t) = \langle p_{T_1}(t)\rangle \langle p_{\tau_C}(t)\rangle, \quad (24)$$

as measured during the mixing time *for this case* factorizes into the terms defined in Eq. (22). From Fig. 6 it is seen that for the uncorrelated scenario the decay times of the modified correlation function, $\tau_2$, do indeed not depend on $t_B$. In the uncorrelated case, this results is independent of the shape of the $\tau_C$ and $T_1$ distributions.

For the simple correlated scenarios of Eq. (18), we started from the same $T_1$ distribution, Eq. (23b), and implemented a positive correlation via $\tau_C = f_C T_1$ and anticorrelation with $\tau_C = f_A / T_1$. These relationships between $\tau_C$ and $T_1$ are graphically depicted in the inset of Fig. 6 as cases 1 and 5, respectively. The simulation data presented in Fig. 6 were obtained with $f_C = 10^{-1}$ and $f_A = 10^5$ s$^2$. For both scenarios the $\tau_2$ values do depend on the build-up time $t_B$ and show opposite, albeit slightly asymmetric, trends. This makes it easy to distinguish the positively correlated, the uncorrelated, and the anticorrelated scenarios. The slight asymmetry is due to the fact that the $T_1$ filter acts from the longtime side upon the asymmetric $T_1$ distribution. For long build-up times the weighting of the $\beta$ relaxation times does not matter and the time scales $\tau_2$ should approach each other, as is confirmed in Fig. 6.

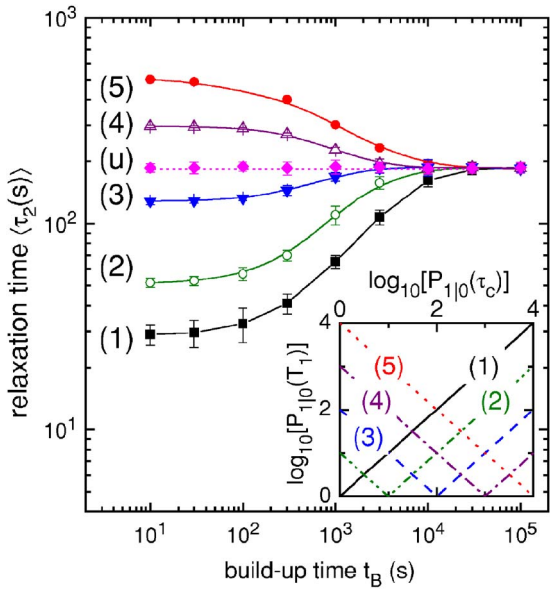


FIG. 6. (Color online) Effective correlation times $\tau_2$ as a function of the build-up time $t_B$. The time constants were obtained from Kohlrausch fits to the simulated polarization $\langle p_{T_1}(t) p_{\tau_C}(t)\rangle$. Since the distribution of Eq. (23) was used, the fits were not always perfect as reflected by the error bars. The symbols represent the results of the simulations as described in the text. The lines are drawn to guide the eye. For the uncorrelated case ($u$) no dependence of $\tau_2$ on $t_B$ was found. Other scenarios, numbered 1 through 5, are depicted in the inset, which shows the relation between $\tau_C$ and $T_1$ analogous to the "connectivity matrix" depicted in Fig. 2. In the main figure the corresponding numerical results for $\tau_2$ are shown.

Only in the slow motion limit is the relaxation time a monotonous function of the spin-lattice relaxation time. Let us assume that some $\beta$ relaxation times are faster than the time scale $\tau_x = 0.61/\omega_L$ corresponding to the $T_1$ minimum. For typical external fields $\tau_x$ is a few nanoseconds. We can mimic this situation by a nonmonotonous relationship such as that sketched as case 2 in the inset of Fig. 6. In physical terms, the particular relationship chosen there implies that 25% of all molecules are faster than $\tau_x$. In typical experimental situations this fraction will be much smaller. The numerical results in Fig. 6 show that even with this large fraction of fast molecules the trend is dominated by the time constants $\tau_C$ which are proportional to $T_1$. The results of further nonmonotonous scenarios are included in Fig. 6 and show the continuous evolution of the trends. Remarkably the asymmetry as discussed above leads to a minor effect in $\tau_2$ for the V-shaped scenario 3.

For the correlated case 1, we checked how an increase of the distribution widths alters the results. Choosing distributions with widths of four rather two decades, one sees from Fig. 7(a) that $\tau_2$ changes over a much wider range than before. Since qualitatively the trend is the same as for the narrower distributions, we return to work with the narrow distributions for the following examples.

The impact of an exchange process in the presence of correlations was also tested. From the results depicted in

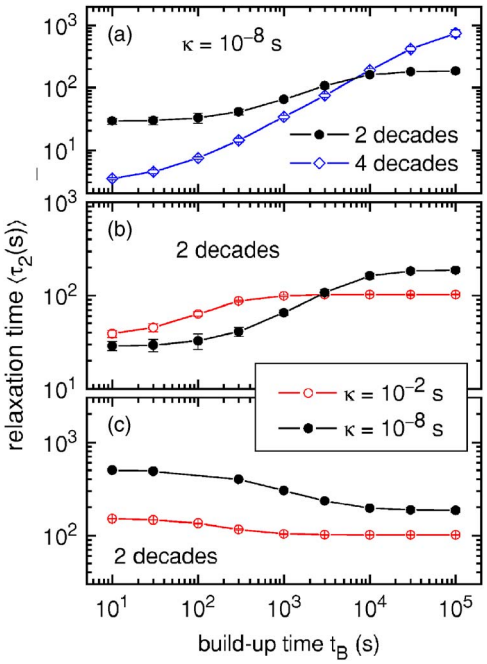


FIG. 7. (Color online) The uncorrelated scenario is shown in frame (a) for two different distribution widths. Results for positive correlations and the impact of exchange within the $\tau_C$ and $T_1$ distributions are presented in (b) for distributions which are two decades wide. The same but for negative correlations in (c). The different symbols correspond to different exchange rates $\kappa$. The numerical values of $\kappa=10^{-8}$ s or $\kappa=10^{-2}$ s were chosen in order to simulate the cases of negligible or significant exchange during $t_m$ and/or $t_B$, respectively.

Figs. 7(b) and 7(c), one recognizes that exchange within the $T_1$ and $\tau_C$ distributions reduces the strength of the trends but does not change them. Thus our simulations suggest that exchange can alter the trends only quantitatively but not qualitatively. This is understandable since, depending on the relation of $\kappa$ to the upper and lower limits of the initial distributions chosen for $\tau_C$ and for $T_1$, we find various degrees of narrowing of these distributions. Such "motionally narrowed," effective distributions are well known, in particular in the context of magnetic resonance [53]. Also for the uncorrelated scenario an increase of the exchange rate within the $\tau_C$ distribution reduces the absolute value of the otherwise $t_B$ independent $\tau_2$ (not shown).

Finally we checked, for a positively correlated scenario, the degree of deviation from the factorization given by Eq. (24). In Fig. 8 we show examples for the time domain signals $\langle p_{T_1}(t)\rangle$, $\langle p_{\tau_C}(t)\rangle$, and $\langle p(t)\rangle$ obtained with $f_C=10^{-1}$ and the distribution given by Eq. (23b). For the simulation presented in Fig. 8 a long build-up time ($t_B=10^4$ s) and a small exchange rate ($\kappa=10^{-6}$ s) were chosen, since these values should give rise to the most pronounced violation of the factorization. However, it is seen from the near equality of the "experimental" function $\langle p_{T_1}(t)p_{\tau_C}(t)\rangle$ (solid line in Fig. 8) with the product $\langle p_{T_1}(t)\rangle\langle p_{\tau_C}(t)\rangle$ (dash-dotted line) that even under these conditions the factorization of Eq. (24) represents a rather good approximation.

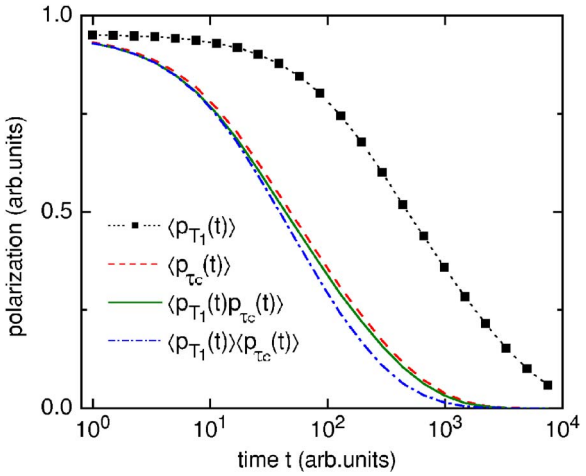


FIG. 8. (Color online) Correlation functions for a positively correlated scenario as simulated at the indicated 25 equally spaced points on a logarithmic time axis, here mostly represented as lines. The modified spin-lattice relaxation $\langle p_{T_1}(t)\rangle$ (black, dotted line) is identical with the expectation based on Eq. (10). The correlation function $\langle p_{\tau_C}(t)\rangle$ (red, dashed line), which is free from any spin-relaxation effects, is not accessible in a laboratory experiment. The experimentally relevant function $\langle p_{T_1}(t)p_{\tau_C}(t)\rangle$ (green, solid line) is almost identical with the product $\langle p_{T_1}(t)\rangle\langle p_{\tau_C}(t)\rangle$ (blue, dash-dotted line). This agreement shows that the factorization of Eq. (24) represents a good approximation.

## VI. CONCLUDING REMARKS

To summarize, we first qualitatively developed the idea of how to describe a possible connection of the primary with the secondary relaxation near the glass transition of supercooled liquids. Then we proposed an NMR technique, spin-lattice relaxation weighted stimulated-echo spectroscopy, in order to implement the idea. Here first the longitudinal magnetization is destroyed, then allowed to at least partially build up again in a fashion which is sensitive to the secondary relaxation, and finally tested on the time scale of the primary relaxation. The time constants $\tau_2$ that describe the orientational decorrelation in the last part of this experiment will then in general depend on the time $t_B$ that was chosen for buildup.

We also discussed in detail possible difficulties that can arise when evaluating experimental data. Then we derived a general theoretical framework in order to describe such experiments quantitatively in the presence of correlation effects. Using numerical simulations we analyzed these expressions and also generalized them to include the effect of dynamical exchange processes. This allowed us to demonstrate how, in a straightforward way, the dependence of $\tau_2$ on $t_B$ can be used to signal whether or not and then in which way the time constants of the primary and the secondary relaxation are related to one another. However, the various dependences on the shape of the corresponding distributions, on the exchange constant, and on various other factors that we have discussed above enter into how $\tau_2$ exactly depends on $t_B$. Since detailed information on these factors will usually not be available from experiments it will be hard to

interpret $\tau_2(t_B)$ quantitatively beyond extracting the type of correlation. In an accompanying paper, we show experimentally for several glass formers that a positive correlation between the spin-lattice relaxation times and the primary correlation times exists [27].


## ACKNOWLEDGMENTS

We thank M. Winterlich, A. Nowaczyk, and G. Hinze for stimulating discussions. This project was financially supported by the Deutsche Forschungsgemeinschaft within the Graduiertenkolleg 298.



[1] C. A. Angell, Science **267**, 1924 (1995).
[2] R. Böhmer, G. Diezemann, G. Hinze, and E. Rössler, Prog. Nucl. Magn. Reson. Spectrosc. **39**, 191 (2001).
[3] F. Fujara, B. Geil, H. Sillescu, and G. Fleischer, Z. Phys. B: Condens. Matter **88**, 195 (1992).
[4] G. P. Johari and M. Goldstein, J. Chem. Phys. **53**, 2372 (1970).
[5] P. Lunkenheimer, U. Schneider, R. Brand, and A. Loidl, Contemp. Phys. **41**, 15 (2000).
[6] A recent dielectric experiment indicated that neither secondary relaxations nor excess contributions seem to be present in the supercooled plastic crystal ortho-carborane, see R. Brand, P. Lunkenheimer, U. Schneider, and A. Loidl, Phys. Rev. Lett. **82**, 1951 (1999).
[7] A. Döß, M. Paluch, H. Sillescu, and G. Hinze, Phys. Rev. Lett. **88**, 095701 (2002); A. Döß, M. Paluch, H. Sillescu, and G. Hinze, J. Chem. Phys. **117**, 6582 (2002).
[8] M. Vogel and E. A. Rössler, J. Chem. Phys. **114**, 5802 (2001); M. Vogel, P. Medick, and E. A. Rössler, Annu. Rep. NMR Spectrosc. **56**, 201 (2005).
[9] T. Blochowicz, A. Kudlik, S. Benkhof, J. Senker, E. Rössler, and G. Hinze, J. Chem. Phys. **110**, 12011 (1999).
[10] R. Böhmer and F. Kremer, in *Broadband Dielectric Spectroscopy*, edited by F. Kremer and A. Schönhals (Springer, Berlin, 2002), pp. 625–684.
[11] Field-cycling NMR techniques provide a more direct way to measure the frequency dependence of $T_1$ over a broad range; see, e.g., F. Noack, S. Becker, and J. Struppe, Annu. Rep. NMR Spectrosc. **33**, 1 (1996); F. Kimmich and E. Anoardo, Prog. Nucl. Magn. Reson. Spectrosc. **44**, 257 (2004).
[12] K. L. Ngai and M. Paluch, J. Chem. Phys. **120**, 857 (2004); C. M. Roland, S. Hensel-Bielowka, M. Paluch, and R. Casalini, Rep. Prog. Phys. **68**, 1405 (2005).
[13] E. Donth, *The Glass Transition: Relaxation Dynamics in Liquids and Disorder Materials* (Springer, Berlin, 2001).
[14] T. Pakula, in *Broadband Dielectric Spectroscopy*, edited by F. Kremer and A. Schönhals (Springer, Berlin, 2002), pp. 597–623, and references cited therein.
[15] J. Leisen, K. Schmidt-Rohr, and H. W. Spiess, Physica A **201**, 79 (1993).
[16] A. S. Kulik, H. W. Beckham, K. Schmidt-Rohr, D. Radloff, U. Pawelzik, C. Boeffel, and H. W. Spiess, Macromolecules **27**, 4746 (1994).
[17] G. Diezemann, U. Mohanty, and I. Oppenheim, Phys. Rev. E **59**, 2067 (1999).
[18] G. Williams, Trans. Faraday Soc. **62**, 2091 (1966).
[19] J. Köplinger, G. Kasper, and S. Hunklinger, J. Chem. Phys. **113**, 4701 (2000).
[20] K. Schmidt-Rohr and H. W. Spiess, Phys. Rev. Lett. **66**, 3020 (1991).
[21] M. T. Cicerone and M. D. Ediger, J. Chem. Phys. **103**, 5684 (1995).
[22] B. Schiener, R. Böhmer, A. Loidl, and R. V. Chamberlin, Science **274**, 752 (1996).
[23] X. H. Qiu and M. D. Ediger, J. Phys. Chem. B **107**, 459 (2003).
[24] W. Schnauss, F. Fujara, K. Hartmann, and H. Sillescu, Chem. Phys. Lett. **166**, 381 (1990).
[25] H. Wagner and R. Richert, J. Non-Cryst. Solids **242**, 19 (1998).
[26] R. Richert, Europhys. Lett. **54**, 767 (2001).
[27] A. Nowaczyk, B. Geil, G. Hinze, and R. Böhmer, following paper, Phys. Rev. E **74**, 041505 (2006).
[28] R. Böhmer, G. Diezemann, B. Geil, G. Hinze, A. Nowaczyk, and M. Winterlich, Phys. Rev. Lett. **97**, 135701 (2006).
[29] N. Bloembergen, E. M. Purcell, and R. V. Pound, Phys. Rev. **73**, 679 (1948).
[30] Since the molecular excursions differ for the $\alpha$ and the $\beta$ relaxations, in a strict treatment we should introduce two coupling constants $K_\alpha$ and $K_\beta$. However, since in the present case the $\beta$ process dominates the spin-lattice relaxation by far, no subscript will be used.
[31] Here we use $J(\omega)=(2/5)(\tau/1+\omega^2\tau^2)$ corresponding to a presence of a single correlation time $\tau$ and an isotropic reorientation process.
[32] If one would have to take into account a distribution of correlation times or an intrinsically non-Lorentzian spectral density, then the Cole-Davidson spectral density $J_{\mathrm{CD}}(\omega)=\frac{2}{5}\omega^{-1}(1+\omega^2\tau^2)^{-\beta_{CD}/2}\sin[\beta_{CD}\arctan(\omega\tau)]$ is often chosen. With a typical exponent of $\beta_{\mathrm{CD}}=0.5$, say, Eq. (2) would have to be replaced by $1/T_1\sim(4K/5\omega)[1/(\omega\tau)^{0.5}]$. Again, using a correlation time of a few $\mu$s the corresponding $T_1$ is separated from it by about five decades. Recognizing that $\beta$ relaxations are anisotropic, the effective coupling is considerably smaller than $K$. This implies a larger separation of time scales than discussed so far. It should be noted that in the present context Eq. (2) is more appropriate since the basic correlation functions can be assumed to be exponential in nature.
[33] G. Diezemann and W. Schirmacher, J. Phys.: Condens. Matter **2**, 6681 (1990).
[34] W. Schnauss, F. Fujara, and H. Sillescu, J. Chem. Phys. **97**, 1378 (1992).
[35] N. G. van Kampen, *Stochastic Processes in Physics and Chemistry* (North Holland, Amsterdam, 1992).
[36] R. Böhmer, G. Hinze, G. Diezemann, B. Geil, and H. Sillescu, Europhys. Lett. **36**, 55 (1996).
[37] In fact for some descriptions, the introduction of an exchange process separate from the primary one is not required, see G. Diezemann, J. Chem. Phys. **107**, 10112 (1997).
[38] B. Geil and G. Hinze, Chem. Phys. Lett. **216**, 51 (1993).

[39] This sets the ultimate low-temperature limit for our technique. It is reached when dipolar flip-flop processes among the spins start to dominate the magnetization recovery. The corresponding exchange processes, usually termed spin-diffusion, are well understood in deuteron systems, see D. Suter and R. R. Ernst, Phys. Rev. B **32**, 5608 (1985); G. Diezemann and H. Sillescu, J. Chem. Phys. **103**, 6385 (1995), and references cited therein.

[40] The replacement of the saturation comb by an initial inversion pulse can increase the sensitivity of the experiment by a factor of 2. However, this option was not used in the present work because not employing saturation techniques would increase the measuring time considerably. Furthermore, an initial inversion pulse leads to a crossover type of experiment [see, e.g., R. Böhmer, B. Schiener, J. Hemberger, and R. V. Chamberlin, Z. Phys. B: Condens. Matter **99**, 91 (1995); *ibid.* **99**, 624 (1996)] which can present further complications.

[41] S. Sen and J. F. Stebbins, Phys. Rev. Lett. **78**, 3495 (1997) recorded spectra employing various delay times subsequent to saturation in their study of a supercooled nitrate melt. However, since the nonexponential magnetization recovery of their sample was due to structural relaxation, they probed the heterogeneity of the primary relaxation rather than a possible correlation between primary and secondary relaxation processes.

[42] K. Schmidt-Rohr and H. W. Spiess, *Multidimensional Solid-State NMR and Polymers*, (Academic, London, 1994).

[43] This limit of the angular jump correlation functions is discussed more thoroughly in Ref. [2].

[44] H. Sillescu, J. Non-Cryst. Solids **243**, 81 (1999).

[45] R. Böhmer, R. V. Chamberlin, G. Diezemann, B. Geil, A. Heuer, G. Hinze, S. C. Kuebler, R. Richert, B. Schiener, H. Sillescu, H. W. Spiess, U. Tracht, and M. Wilhelm, J. Non-Cryst. Solids **235-237**, 1 (1998).

[46] However, in some stimulated-echo experiments nonexponential spin-lattice relaxation occurred. An example is Ref. [8] where the $\beta$ relaxation was studied in the glassy state of toluene and various polymers.

[47] We performed some test experiments along the lines described in Ref. [15], but were unable to recover the conventionally measured spin-lattice curve by operating the stimulated-echo weighted spin-lattice relaxation experiment in the limit of a vanishing low-pass filter efficiency. We attribute this difference to spurious filtering arising from the use of finite evolution times in these experiments and to the fact that a stimulated-echo filter also involves filtering with respect to spin-lattice relaxation. In any case the experimental technique dealt with in the remainder of the present article and in Ref. [27] is the more sensitive and hence from this perspective the preferred one since the stimulated-echo decay is by far more nonexponential as compared to the magnetization recovery. For these reasons the "inverse" experiment of Ref. [15] was not further pursued for the present work.

[48] A nondecaying cos-cos function provides another special case for which the factorization implied by Eq. (8) is justified. This is exploited in Ref. [27].

[49] Since it is clear that $P_{1|0}(R_1)$ and $P_{1|0}(\tau_C)$ denote different functions, for convenience we both call them $P_{1|0}$ in the present article.

[50] S. Wefing and H. W. Spiess, J. Chem. Phys. **89**, 1234 (1988).

[51] Equation (14) implicitly assumes that $R_1$ is the independent variable. Alternatively and equivalently, we could have formulated this and the following equations with the view that $\tau_C$ is the independent variable.

[52] It should be realized that $f_C$ connects the $\alpha$ with the $\beta$ process. Hence $f_C$ is *not* a constant that should be associated with Eq. (2). There time constants relating to the *same* process are involved.

[53] P. W. Anderson and P. R. Weiss, Rev. Mod. Phys. **25**, 269 (1953).